Stabilization of coherent breathers in perturbed Hamiltonian coupled oscillators

Panayotis Panayotaros[†], Alejandro Aceves[††]

[†] Depto. Matemáticas y Mecánica, I.I.M.A.S.-U.N.A.M., Apdo. Postal 20–726, 01000 México D.F., México
Tel.(55) 5622-3600, Fax (55) 5622-3564, e-mail: panos@mym.iimas.unam.mx

[††] Department of Mathematics, Southern Methodist University, Dallas TX 75275

August 30, 2011

Abstract

We propose and study a type of non-Hamiltonian, power-preserving perturbation of Hamiltonian systems of nonlinear coupled oscillators with a global phase invariance symmetry. Our results highlight the role of non-conservative perturbations in selecting a preferred dynamically attracting mode which can be chosen to be highly coherent. The proof of principle described above should be of interest for optical systems such as fiber laser arrays whose objective is to produce high power coherent light

1 Introduction

Nonlinear dynamics described by Hamiltonian systems appear in many disciplines in science and engineering. In the field of nonlinear optics and photonics, many experiments on light propagating in waveguides are modeled effectively by Hamiltonian systems. Examples include the propagation of pulses in optical fibers and light localization in coupled waveguide arrays. Of equal relevance to nonlinear optics are non-conservative systems, the most important being the laser. Here the dynamical balance of linear and nonlinear conservative and non-conservative properties lead to attractors representing the lasing state. Finally in some instances, including those mentioned above, one can improve existing models to account for small effects such as losses, higher order nonlinearities or dispersion. Here, much has been learned from the theory of perturbed Hamiltonian systems.

The last few years have witnessed intensive research activity in the area of fiber laser arrays [1]. The advance in the technology and fabrication of optical fibers, driven by the application in communications, has led, as a by-product, to a new class of lasers where outputs of several ideally identical fiber amplifiers are coupled to produce high power *coherent* beams. It is precisely achieving high coherence that is the most challenging part in designing fiber lasers. Beam combining can be done passively or actively, with the earlier one being simpler to implement. Most passive beam combining schemes are based on linear optical elements and the principle behind the design is one of mode selectivity [2, 3, 4, 5], so that the lasing super-mode is one of N-coherently combined fields.

So far in all instances, the literature shows that coherence eventually decreases and is even lost as the number of elements increases [6]. To be precise in characterizing coherence, we introduce the *efficiency* function $\mathcal{E} = |\sum_{k=1}^{N} u_n|/\sum_{k=1}^{N} |u_n|$ commonly used in fiber laser arrays. Here u_n are the complex fields that account for the lasing mode. One can see that maximum coherence, corresponding to all fields being in phase, is attained when this function is equal to one.

There has been little effort in considering nonlinear beam combining schemes [7], the main reason being the required high powers on the individual fields. While this indeed constitutes an engineering challenge, we should be reminded of how robust the phenomenon of synchronization in coupled nonlinear oscillators is. Generically, one has that individual out of phase oscillators can lock into an in phase state once a critical power threshold (or nonlinear coupling strength) is achieved [8]. In the context of fiber lasers, we believe it is important to find a similar behavior. It is also true that beam combining models neglect losses; again intuitively one expects losses to be a solely negative factor towards high power output. On the other hand if one can demonstrate enhanced coherence at minimal cost of energy, this trade-off may prove to be of benefit [9]. Here, in general terms, while nonlinearity can produce a robust nonlinear coherent mode, losses and gains can make it a dynamical attractor.

The proposed model is based on the idea of using non-Hamiltonian, power-preserving perturbations of Hamiltonian coupled oscillator systems to drive the perturbed system towards a *breather*. The only assumption is that the Hamiltonian is invariant under global phase change. In the present work breathers are solutions of the form $u_n = e^{-i\omega t} A_n$, with ω real, A_n independent of t (in optics the "time" t represents distance along the optical axis). Breathers are known to exist for a large variety of Hamiltonian systems of interest, and have been studied extensively for discrete NLS equations (in finite and infinite lattices), see e.g. Refs. [13], [12], [14], [18]. Stable breathers, can be obtained by looking for local extrema of the energy over configurations with fixed power. Furthermore, there exist stable, energy-extremizing breathers with $\mathcal{E} = 1$. In Hamiltonian models, stability means that the trajectories remain in the vicinity of the breather. To define a perturbation that makes such a breather into an attractor we first write the Hamiltonian system using a system of coordinates in which the stable breathers become stable fixed points of a suitable equivalent *reduced* Hamiltonian system, see e.g. Ref. [10], ch. 4.3, for a general theory of reduction. We then add a term that preserves the stable equilibrium of the reduced Hamiltonian system and turns it into a sink of the perturbed reduced system. Such a perturbed system cannot be Hamiltonian but preserves the power automatically.

We remark that breathers have been studied extensively, especially in connection to localization in nonlinear lattices, and they are often also referred to as localized modes, discrete solitons, etc.. Localization does not enter explicitly in the definition of breathers used here, and we can also have breathers in linear or weakly nonlinear systems, see e.g. [16] on the continuation of breathers as we vary a nonlinearity parameter. Using this rather general (or more mathematical) notion of breather we see that we can stabilize $\mathcal{E} = 1$ breathers with different spatial characteristics, depending on the system and the non-Hamiltonian perturbation we use. We show examples of stabilization of spatially localized breathers in systems with both strong and weak nonlinearity, and we also stabilize spatially "delocalized" breathers, e.g. ones for which all sites have the same amplitude. While the theory behind stabilization is local, we show many examples of breathers that attract trajectories that start far from the vicinity of the breather. We also see trajectories that start far from an attracting breather and converge to a more complicated attractor.

In Section 2 we describe the reduced phase space (see [16], [17]), and discuss perturbations that stabilize breathers. We propose perturbations expected to stabilize energy-extremizing coherent breathers with real, sign-definite amplitudes in all models having such breathers. Essentially, these terms "push" the trajectories towards local maxima or minima of the energy of the unperturbed reduced Hamiltonian system and can either decrease or increase the energy of the system, e.g. they dissipate (add) energy if we start in the vicinity of a local minimum (maximum) of the energy. In Section 3 we test these ideas numerically on one-dimensional discrete NLS equations with cubic and saturable nonlinearities. We also use different linear couplings and boundary conditions. In addition to verifying the stabilization effect for initial conditions in the vicinity of many coherent breathers, we also see cases where the breather attracts trajectories that start far from it. (The change in energy can be large in such cases.) Such phenomena were seen for weakly nonlinear lattices with Dirichlet boundary conditions, and also for periodic boundary conditions with both small and large nonlinearity. The attracting coherent breather can be also localized; attraction seems more robust in weakly nonlinear lattices with a localized potential term.

2 Reduction and attracting breathers in perturbed Hamiltonian systems

We consider a Hamiltonian system in $\mathbf{C}^N$ of the form

$$\dot{u}_n = -i\frac{\partial H}{\partial u_n^*}, \quad n \in \{1, \ldots, N\} \tag{2.1}$$

and assume that the Hamiltonian H is invariant under the global phase change $u_n \mapsto e^{i\phi}u_n$, $n = 1, \ldots, N$, where ϕ is independent of n, so that $[H, P] = 0$, with $P = \sum_{n=1}^N |u_n|^2$ the *power*, and $[\cdot, \cdot]$ the Poisson bracket defined by (2.1). Define polar coordinates J_n, and ϕ_n, by $u_n = \sqrt{J_n}e^{i\phi_n}$. Also define the coordinates I_n, and θ_n by

$$\theta_n = \phi_{n+1} - \phi_n, \quad n = 1, \ldots, N-1, \quad \theta_N = \sum_{n=1}^N \phi_n \tag{2.2}$$

$$J_1 = I_1 + I_N, \quad J_n = I_n - I_{n-1} + I_N, \quad n = 2, \ldots, N-1, \quad J_N = I_N - I_{N-1}. \tag{2.3}$$

In vector notation we write (2.2) as $\theta = M\phi$. Then (2.3) implies $I = (M^{-1})^T J$. The matrix M^{-1} is given in (2.22) below. Equation (2.1) is then

$$\dot{I}_n = \frac{\partial H}{\partial \theta_n}, \quad \dot{\theta}_n = -\frac{\partial H}{\partial I_n}, \quad n \in \{1, \ldots, N\}. \tag{2.4}$$

The Poisson bracket of H and $P = \sum_{k=1}^N J_k$ vanishes, therefore

$$[H, P] = 2\sum_{k=1}^N \frac{\partial H}{\partial \phi_k}\frac{\partial P}{\partial J_k} = 2\sum_{k=1}^N \frac{\partial H}{\partial \phi_k} = 0. \tag{2.5}$$

Also, the definition of the θ_j in (2.2) implies $\partial_{\theta_N}\phi_k = N^{-1}$, so that (2.5) yields

$$\frac{\partial H}{\partial \theta_N} = \sum_{k=1}^N \frac{\partial H}{\partial \phi_k}\frac{\partial \phi_k}{\partial \theta_N} = \frac{1}{N}\sum_{k=1}^N \frac{\partial H}{\partial \phi_k} = 0. \tag{2.6}$$

The Hamiltonian H is therefore independent of θ_N, and (2.4) becomes

$$\dot{I}_n = \frac{\partial H}{\partial \theta_n}, \quad \dot{\theta}_n = -\frac{\partial H}{\partial I_n}, \quad n \in \{1, \ldots, N-1\}, \quad \dot{I}_N = 0, \quad \dot{\theta}_N = -\frac{\partial H}{\partial I_N}. \tag{2.7}$$

Since $\dot{I} = 0$, we can set $I_N = c$, and solve the first $2(N-1)$ equations with $H = h_c$, where h_c is H with the variable I_N set to the constant value c. We also have $I_N = N^{-1}P$ so that c is interpreted as the power per site. The first $2(N-1)$ equations of (2.7) are referred to as the *reduced system*. Once they are solved, the RHS of the equation for $\dot{\theta}_N$ depends on the $I_n(t)$, $\theta_n(t)$, $n = 1, \ldots, N-1$, and the constant c, and can be integrated to find $\theta_N(t)$. Thus the reduced system determines the nontrivial part of the evolution completely. Finally we may write (2.7) as

$$\dot{I}_n = \frac{\partial h_c}{\partial \theta_n}, \quad \dot{\theta}_n = -\frac{\partial h_c}{\partial I_n}, \quad n \in \{1, \ldots, N-1\}, \quad \dot{I}_N = 0, \quad \dot{\theta}_N = -\frac{\partial H}{\partial I_N}. \tag{2.8}$$

The above system is well defined for I_k satisfying $J_n > 0$, $n = 1, \ldots, N$, in (2.3), and some care is needed when a trajectory passes from a point with $J_n = 0$ for some n. This is discussed further below. More information on the underlying theory is in Remark 2.1 and in Ref. [17].

We can instead consider the modified system

$$\dot{I}_n = \frac{\partial h_c}{\partial \theta_n} + a_n, \quad \dot{\theta}_n = -\frac{\partial h_c}{\partial I_n} + b_n, \quad n \in \{1, \ldots, N-1\}, \quad \dot{I}_N = 0, \quad \dot{\theta}_N = -\frac{\partial H}{\partial I_N}, \tag{2.9}$$

with a_n, b_n functions of I_n, θ_n, $n = 1, \ldots, N-1$. Such a perturbation of (2.8) will clearly preserve I_N and the power $P = N^{-1}I_N$. Here we want to choose a_n, b_n so that certain (selected) fixed points of the reduced Hamiltonian system become attractors. The fixed points of the reduced system correspond to solutions of (2.1) that have the form $u_n = e^{-i\omega t}A_n$, ω real, A_n independent of t, i.e. the *breather* solutions. We consider the case of static solutions of the reduced system that are the local extrema of the reduced Hamiltonian h_c, equivalently local extrema of H over all configurations with power $P = Nc$. Such extrema exist under very general conditions and are nonlinearly stable solutions of the reduced system, see Remark 2.1.

Perturbations that make such fixed points local attractors should be abundant. For example we can add to the reduced system a small multiple of the gradient of h_c. To see this, consider the following equivalent model problem. Let $z = [I_1, \ldots, I_{N-1}, \theta_1, \ldots, \theta_{N-1}] \in \mathbf{R}^{2N-2}$, let J be the symplectic matrix in $\mathbf{R}^{2N-2}$. Let f be a smooth function defined in a neighborhood U of the origin in $\mathbf{R}^{2N-2}$ that has the origin as an isolated maximum or minimum. Also assume that $f(\mathbf{0}) = 0$. Consider now the perturbed system

$$\dot{z} = J\nabla f + \epsilon \nabla f, \tag{2.10}$$

with ϵ real. By the assumptions on f we have $\nabla f(\mathbf{0}) = \mathbf{0}$ so that the origin is an isolated fixed point for all ϵ. The first term represents the Hamiltonian part of the system, with f the Hamiltonian. For $\epsilon = 0$ the origin is a stable fixed point of a Hamiltonian system, and trajectories stay in the vicinity of the origin for all times. The perturbation has the special form of gradient of f and we can choose the sign of ϵ so that the gradient term pushes the trajectories towards the origin. If for example the origin is a maximum of f, then f is negative near the origin and we can choose $\epsilon > 0$. In fact $\Lambda = -f$ is positive near the origin and

$$\frac{d}{dt}\Lambda = -(\nabla f)^T \dot{z} = -(\nabla f)^T J \nabla f - \epsilon (\nabla f)^T \nabla f = -\epsilon ||\nabla f||^2, \tag{2.11}$$

where $(\nabla f)^T J \nabla f$ vanishes identically. Thus for $\epsilon > 0$ the "distance" function Λ is strictly decreasing for $z \neq 0$, and the trajectories must approach the origin. If the origin is a minimum we use $\epsilon < 0$, then $\Lambda = f$ also decreases.

The specific examples we discuss in the next section follow from a related heuristic argument. We want the same scenario of an extremum of the Hamiltonian part, but will examine instead what happens when the model is given by a linear Hamiltonian part plus a linear perturbation. The notation is as in the first example and we let $f = \pm\frac{1}{2} z^T \mathcal{H} z$, where $\mathcal{H}$ is a positive definite $2(N-1) \times 2(N-1)$ real matrix. Let A be a $2(N-1) \times 2(N-1)$ real matrix. We consider the system

$$\dot{z} = J\nabla f + \epsilon A z = J\mathcal{H} z + \epsilon A z, \tag{2.12}$$

with ϵ real. For $A = \mathcal{H}$ we have a linear version of the first example with a maximum (minimum) of f for $+$ $(-)$, but we here consider a more general perturbation. Then for $\Lambda = \pm f$ (> 0 for $z \neq 0$) we have

$$\frac{d}{dt}\Lambda = \epsilon z^T \mathcal{H} A z. \tag{2.13}$$

For $\epsilon < 0$, and $\mathcal{H}A$ positive definite we have $\dot{\Lambda} < 0$ as in the first example. We may also try more general A for which $z^T \mathcal{H} A z > 0$ for all z not in some nontrivial subspace V. If V is not an invariant subspace of (2.12) then Λ should also decrease monotonically in time and the trajectories will eventually go to the origin. In some cases of such more general A we can also establish linear stability by examining the eigenvalues of $J\mathcal{H} + \epsilon A$. Observe also that the same A will work for both maxima and minima: when we start near a maximum (minimum) the energy increases (decreases).

To indicate the use of this type of dissipation we first consider the 2−site system, which in fact highlights the basic ideas. We have $J_n = |u_n|^2$, $n = 1, 2$, and

$$\theta_1 = \phi_2 - \phi_1, \quad \theta_2 = \phi_1 + \phi_2, \quad I_1 = \frac{1}{2}(J_1 - J_2), \quad I_2 = \frac{1}{2}(J_1 + J_2). \tag{2.14}$$

The Hamiltonian H depends on I_1, I_2, θ_1, and we set $I_2 = c$. Also $h_c(I_1, \theta_1) = H(I_1, \theta_1, c)$. For the cubic discrete NLS (see next section) we have

$$h_c = -\delta\sqrt{c^2 - I_1^2}\cos\theta_1 + I_1^2. \tag{2.15}$$

The domain of I_1 is obtained by requiring $J_n > 0$, $n = 1, 2$, which yields $|I_1| < c$. The fixed points of the reduced system for I_1, θ_1 are seen from the contour plot of h_c in Figure 1. We have chosen $\delta < 0$, with $|\delta| < 2c$. We see three stable fixed points, two at $\theta_1 = 0$, and another one at $\theta = \pi$. (For $|\delta| \geq 2c$ the three fixed points on $\theta_1 = 0$ coalesce.) We will try to make the stable fixed points on $\theta_1 = 0$ into attractors by considering the perturbed reduced system

$$\dot{I}_1 = \frac{\partial h_c}{\partial \theta_1}, \quad \dot{\theta}_1 = -\frac{\partial h_c}{\partial I_1} - \alpha\theta_1, \quad \alpha > 0. \tag{2.16}$$

Intuitively, we are pushing towards $\theta_1 = 0$, or along the gradient of $-\frac{1}{2}\theta_1^2$. The choice of the sign of α follows from previous knowledge that the two fixed points at $\theta_1 = 0$ are maxima of h_c. In this problem the fixed points and the eigenvalues of the linearization around them can be calculated explicitly. The eigenvalues are

$$\lambda = -\frac{\alpha}{2} \pm \frac{\sqrt{\Delta}}{2}, \quad \Delta = \alpha^2 - 2|\delta|\left(4c^2 - |\delta|^2\right). \tag{2.17}$$

For $\alpha > 0$ sufficiently small, and $|\delta| \geq 2c$, one has asymptotic stability. We note that in the notation of (2.12) the perturbation used here corresponds to

$$A = \begin{bmatrix} 0 & 0 \\ 0 & 1 \end{bmatrix} \tag{2.18}$$

so that the analogue of $\mathcal{H}A$ is not positive definite (also $\alpha = -\epsilon$). If the fixed point we want to stabilize is at $(I_1, \theta_1) = (K, 0)$ one could also add to the equation for $\dot{I}_1$ the term $-\alpha(I_1 - K)$. The fixed point is again seen to be stable. The advantage of using the perturbation of (2.16) is that we do not need to know the fixed point in advance. This is also the case with (2.10), but the perturbation of (2.16) is also independent of the Hamiltonian. Similar considerations apply to the the saturable NLS (see next section), where the 2-site reduced Hamiltonian h_c is

$$h_c = -\delta\sqrt{c^2 - I_1^2}\cos\theta_1 + \log[(1+c)^2 - I_1^2] \tag{2.19}$$

There is a range of $\delta > 0$ where the phase space of (2.19) looks like Figure 1.

We now generalize to larger lattices by considering the perturbed system

$$\dot{I}_n = \frac{\partial h_c}{\partial \theta_n}, \quad \dot{\theta}_n = -\frac{\partial h_c}{\partial I_n} - \alpha g(\theta_n), \quad n \in \{1, \ldots, N-1\}, \quad \dot{I}_N = 0, \quad \dot{\theta}_N = -\frac{\partial H}{\partial I_n}. \tag{2.20}$$

with $\alpha > 0$, and g an odd function with $g'(0) > 0$, e.g. $g(\theta) = \theta$ or $\sin\theta$ (which is also differentiable at π). The assumption is that we have solutions with $\theta_1 = \ldots = \theta_{N-1} = 0$ that are also local extrema of h_c, i.e., we have an extremum that is also positive (modulo global phase change) at all sites. This is something that in many cases is known (e.g. in the cubic DNLS with Dirichlet boundary conditions [16]), and is also reasonable to expect in many situations. For instance, recall results on the positivity of the ground state for the Schrödinger equation. These fixed points are interesting because they correspond to breathers that have maximum *efficiency* $\mathcal{E} = 1$, where we define

$$\mathcal{E} = \frac{|\sum_{k=1}^{N} u_n|}{\sum_{k=1}^{N} |u_n|}. \tag{2.21}$$

Note that $\mathcal{E}$ is constant (≤ 1) along any breather. The added terms in (2.10) and (2.20) are independent of the location of the stable fixed point. The second choice makes an assumption about the angles of the extremum, but does not depend on the model.

Writing the above added terms in the original variables u_k is straightforward. To indicate their form in the case of (2.20) write the definition of the variable θ_j in (2.2) in matrix form as $\theta = M\phi$, with $\theta = [\theta_1, \ldots, \theta_N]$, etc. We have $\phi = M^{-1}\theta$, where

$$(M^{-1})_{ij} = \begin{cases} \frac{1}{N}(-N + j), & i \leq j, \quad i \in \{1, \ldots, N\}, \quad j \in \{1, \ldots, N-1\}, \\ \frac{j}{N}, & i > j, \quad i \in \{1, \ldots, N\}, \quad j \in \{1, \ldots, N-1\}, \\ \frac{1}{N}, & j = N, \quad i \in \{1, \ldots, N\}. \end{cases} \tag{2.22}$$

By (2.20), (2.2), and (2.3), the perturbed equations in the coordinates J_n, and ϕ_n become

$$\dot{J}_n = \frac{\partial H}{\partial \phi_n}, \quad \dot{\phi}_n = -\frac{\partial H}{\partial J_n} - \alpha(M^{-1}\tilde{g})_n, \quad n \in \{1, \ldots, N\}, \tag{2.23}$$

with

$$\tilde{g} = [g(\theta_1), \ldots, g(\theta_N)]^T = [g(\phi_2 - \phi_1), \ldots, g(\phi_N - \phi_{N-1}), g(\phi_1 + \ldots + \phi_N)]^T. \tag{2.24}$$

Then from $u_n = \sqrt{J_n} e^{i\phi_n}$ we have

$$\dot{u}_n = \frac{1}{2} J_n^{-\frac{1}{2}} \dot{J}_n e^{i\phi_n} + \sqrt{J_n} e^{i\phi_n} \dot{\phi}_n, \tag{2.25}$$

so that

$$\dot{u}_n = -i \frac{\partial H}{\partial u_n^*} - \alpha u_n (M^{-1} \tilde{g})_n, \quad n \in \{1, \ldots, N\}, \tag{2.26}$$

i.e. compare to (2.1). For instance the choice $g(\theta) = \sin\theta$, and (2.24) lead to

$$\tilde{g}_j = \begin{cases} |u_{j+1}|^{-1} |u_j|^{-1} (u_{j+1} u_j^* - c.c.), & j = 1, \ldots, N-1, \\ |u_1|^{-1} \ldots |u_N|^{-1} (u_1 \ldots u_N - c.c.), & j = N. \end{cases} \tag{2.27}$$

The added term is (2.26) is obtained readily from (2.27), and (2.22).

The evolution of (2.26) conserves the power P but will not in general conserve H.

Also notice that the added term of (2.27) has singularities when one of the u_j vanishes. This is also the case for the choice $g(\theta) = \theta$ used in (2.16). In both cases the singularity is due to the fact that ϕ_j is not defined when $u_j = 0$, i.e. the change to planar polar coordinates is singular at the origin for each u_j. We can avoid the singularity by multiplying g by a smooth function of the I_j, $j = 1, \ldots, N-1$, that is constant in most of the region $J_k > 0$, $k \in \{1, , \ldots, N\}$, where we expect to find the breather, and vanishes at its boundaries. In practice it appears sufficient to set the added term to zero when the trajectory is inside some small neighborhood U of the singular set. The added term is then well defined everywhere but discontinuous. By choosing U appropriately we see that the trajectories remain outside U for all times.

Remark 2.1 *The explicit reduced phase space construction above has an abstract counterpart in the theory of symplectic reduction. Following the general theory, see Ref. [10], ch. 4.3, the reduced phase space for the systems we are considering is* $\mathbf{CP}^{N-1}$*, a compact manifold, where smooth functions have at least a maximum and and a minimum. The* θ_k*, and* J_k *of (2.2), (2.3) define a system of coordinates on* $\mathbf{CP}^{N-1}$ *for which Hamilton's equations preserve their standard form. Some breathers are near, or at the set where the coordinates we are using are not defined. A system that seems to avoid these problems is the system of homogeneous coordinates, see e.g. Ref. [15], p. 26.*

3 Examples from discrete NLS equations

The above ideas were applied to discrete nonlinear Schrödinger (DNLS) equations in a one-dimensional N-site lattice. These systems are relevant to several applications such as laser beam combining, and waveguide arrays. We considered equations (2.26) with Hamiltonians of the form

$$H = -\delta \sum_{n,m=1}^{N} u_n^* \mathcal{L}_{nm} u_m - \sum_{n=1}^{N} V_n |u_n|^2 + \sum_{n=1}^{N} G(|u_n|), \tag{3.1}$$

where $\mathcal{L}$ is a symmetric real matrix, V_n is real for all n, and G is a real function.

The first term describes a linear coupling between the sites. Examples include the (nearest-neighbor) *Dirichlet Laplacian*, defined by

$$(\mathcal{L}u)_n = \begin{cases} u_{n-1} - 2u_n + u_{n+1}, & n = 2, \dots, N-1, \\ -2u_1 + u_2, & n = 1, \\ u_{N-1} - 2u_N, & n = N, \end{cases} \tag{3.2}$$

and the (nearest-neighbor) *periodic Laplacian*, defined by

$$(\mathcal{L}u)_n = \begin{cases} u_{n-1} - 2u_n + u_{n+1}, & n = 2, \dots, N-1, \\ u_N - 2u_1 + u_2, & n = 1, \\ u_{N-1} - 2u_N + u_1, & n = N. \end{cases} \tag{3.3}$$

Examples that couple more neighbors, such as a five-point Laplacian, are described below.

The second term in (3.1) describes a "potential" for the DNLS (we prefer not to absorb this into the first term).

The third term describes the nonlinearity, and we here restrict our attention to *cubic*, and *saturable* nonlinearities, corresponding to

$$G(|u_n|) = |u_n|^4, \quad \text{and} \quad G(|u_n|) = \log(1 + |u_n|^2) \tag{3.4}$$

respectively. In the absence of the nonlinear term, breathers are eigenvectors of the matrix $\mathcal{L} + V$, i.e. the linear normal modes.

The perturbed Hamiltonian system (2.26) with $g(\theta) = \sin\theta$ was integrated numerically. Results for $g(\theta) = \theta$ are similar. Implementation of (2.26) for arbitrary N is immediate. We also choose a threshold τ and set $g = 0$ if $|u_k| < \tau$ for some $k \in 1, \dots, N$. We saw that τ can be chosen small enough so that no trajectories pass through the region where g vanishes. Thus the discontinuity of g is not seen by the numerical integration, and the singularity of the term g does not seem to cause any difficulties. The choice of τ depends on the breather one wants to stabilize, e.g. if its amplitude at some sites is expected to be small τ must be chosen accordingly small.

Generically, we observed that trajectories of (2.26) with H and g as above indeed converge to breather solutions with $\mathcal{E} = 1$ in a variety of models with cubic and saturable nonlinearities, and with different linear couplings (e.g. Dirichlet and periodic nearest-neighbor Laplacians, higher order Laplacians, etc.) and potentials. For initial conditions near the breather, the results are to be expected by the heuristic analysis of the previous section. In what follows we mainly document parameter ranges and models where convergence is achieved from initial conditions that are far from the breathers. These cases are also simpler to study since we do not need to know the breather in advance. Also, there is no apparent limitation on N although at present we have only considered up to $N = 17$ sites. What follows is an outline of some of the most relevant numerical results.

We first test the ideas above for lattices with $N = 2$, 3. We integrate both the reduced phase space equations (2.20) and (2.26) and see that the results are the same. For instance, we set $N = 3$ and consider (2.20) for the cubic DNLS with Dirichlet Laplacian, with $\delta = -1.2$ and $\alpha = 0.1$.

We integrate from the initial condition $(I_1, \theta_1, I_2, \theta_2) = (-0.78, -0.2, 0.8, 0.15)$, we find that the trajectory converges to $(-0.881129778, 0, 0.881129778, 0)$, a breather computed independently. In further experiments with the same equation with $\alpha = 0.1$, we start further away from the breather, but keep θ_j about the same. For instance, we set $\delta = -2.4$ and integrate from $(I_1, \theta_1, I_2, \theta_2) = (-0.78, -0.2, 0.8, 0.15)$. The trajectory converges to $(-0.602559046, 0, 0.602559046, 0)$, also a known breather. The fact that $\theta_1 = \theta_2 = 0$ implies $\mathcal{E} = 1$. We remark that the attracting breather is known to be a global maximum of the energy, thus its local attractivity is expected.

For larger lattices we integrate (2.26). We first consider *Dirichlet* boundary conditions and vanishing potential, starting from initial conditions that are near an expected breather satisfying $\mathcal{E} = 1$. For instance, as $|\delta|$ is increased both the cubic and the saturable DNLS become closer to being linear and the extremum breather is expected to approach the ground state of the Dirichlet Laplacian. For the nearest-neighbor Dirichlet Laplacian the ground state is known explicitly and is positive at all sites. The initial efficiency can be near unity regardless of the distance from the expected breather, e.g. using initial conditions that have small imaginary parts, and real parts of the same sign. In Figures 2a-b we integrate the saturable DNLS with $N = 17$, $\delta = -5.1$ and $\alpha = 0.1$. In Figures 2a we show $|u_n(0)|$, and $|u_n(100)|$. The trajectory evolves quickly towards a breather with the amplitude profile of $|u_n(100)|$, i.e. we observe that the $|u_j|$, and the phase differences between neighboring sites converge. In Figure 2b (upper curve) we show the evolution of $\mathcal{E}$ in the time interval $[0, 100]$. We see that the attracting breather has $\mathcal{E} = 1$. Note that the initial efficiency is 0.985306583, i.e. high, but the initial condition is relatively far from the breather, i.e. see Figure 2a. The profile of $|u_n(100)|$ in Figure 2a is close to the profile of the ground state of the Dirichlet Laplacian. Convergence to the above breather is also seen from initial conditions that are not in its vicinity and have low initial efficiencies. An example is indicated in Figure 2b (lower curve) where we show the evolution of $\mathcal{E}$ for an initial condition with initial efficiency 0.528646241. The efficiency evolves towards unity, and the trajectory evolves towards a profile similar to that of Figure 2a (the power of the second trajectory is slightly different).

We obtain similar results using an $\mathcal{L}$ that involves coupling with more neighbors and analogous Dirichlet-like boundary conditions. For instance, to couple two nearest neighbors, let

$$(\mathcal{L}u)_n = bu_{n-2} + au_{n-1} + cu_n + au_{n+1} + bu_{n+2}, \quad n = 3, \ldots, N-2, \tag{3.5}$$

and define $\mathcal{L}u$ at the remaining sites by setting the coefficients of the u_n with $n \notin \{1, \ldots, N\}$ to zero in the above formula. The particular recipe for the endpoints is analogous to that of (3.2). Examples we considered include a higher order finite-difference *five-point Dirichlet Laplacian*, with $b = -1/12$, $a = 4/3$, $c = -10/3$, and its perturbation with $b = -4/12$, $a = 4/3$, $c = -10/3$. Integrating the saturable NLS with $N = 17$, $\delta = -5.1$, $\alpha = 0.1$ we see convergence to an $\mathcal{E} = 1$ breather that is similar to the one shown in Figure 2a. Convergence is seen for initial conditions that are far from the breather and have low efficiency. It appears that the convergence is faster for the first of these five-point $\mathcal{L}$.

In the above examples we are in the "weakly nonlinear" regime where the linear coupling parameter is relatively large and the energy is maximized by a breather that is near the ground state of the linear problem. Thus the local attractivity of the breather we see is expected by the theory. The apparent global attractivity is not as well understood, although we expect that in the linear limit the number of possible extrema of the energy is reduced and we see convergence to one of the two global extrema.

A natural question is whether we can have attracting $\mathcal{E} = 1$ breathers that are also localized in space. In principle local attractivity of spatially localized breathers should be possible. One option is to look for localized extremal breathers in weakly nonlinear lattices with a well localized potential. The existence of such breathers is suggested by considering a quadratic Hamiltonian H of (3.1) with $\delta < 0$ and a potential V that has a large negative value at a single site. We expect that to maximize such an H keeping the power fixed we must use a configuration that is localized near the minimum of the potential. In numerical experiments we observe that such localized weakly nonlinear breathers can also attract trajectories that start far from the breather and have small efficiency. For instance Figure 3a shows $|u_n(0)|$, and $|u_n(200)|$ for the saturable DNLS with the five-point Dirichlet Laplacian above, using $N = 17$, $\delta = -4.0$, $\alpha = 0.1$, and a potential V satisfying $V_9 = -10.0$ and $V_n = 0$ for $n \neq 9$. The trajectory converges to a breather with the amplitude profile of $|u_n(200)|$. Evidently we have spatial localization in the vicinity of the potential well. The evolution of $\mathcal{E}$ in the time interval $[0, 200]$, in Figure 3b, also shows that the attracting breather has $\mathcal{E} = 1$. Initially $\mathcal{E} = 0.164688997$, and it is clear that the initial condition is far from the breather.

Another scenario of localization involves small coupling $|\delta|$. We can approximate heuristically this regime by considering the Hamiltonian H of (3.1) with $\delta = 0$ and $V = 0$. We see that the global maximum of the cubic DNLS Hamiltonian and the global minimum of the saturable DNLS Hamiltonian is, in each case, attained by a breather whose amplitude is nonvanishing in only one site (in both cases we extremize keeping the power fixed). For $|\delta|$ sufficiently small we expect nearby localized extremal breathers. Numerical experiments in the regime of small $|\delta|$ show that convergence to the breather requires initial conditions that are relatively near the breather. To see some examples of small $|\delta|$ behavior we considered the cubic NLS with the nearest-neighbor Dirichlet Laplacian, $V = 0$, and $N = 9$, $\delta = -0.2$ and $\alpha = 0.1$. In Figure 4a we show $|u_n(0)|$, and $|u_n(1200)|$. The evolution of $\mathcal{E}$ in the time interval $[0, 1200]$ in Figure 4b indicates that the trajectory converges to the breather slowly in comparison to what is seen above. Initially $\mathcal{E} = 0.784890617$, and we see that the initial condition is relatively localized near the breather. Considering instead the same system with the initial condition $u(0)$ as in Figure 5a, the trajectory does not seem to approach any breather. After a transient of about 1000 the trajectory exhibits an amplitude profile seen in $|u(2000)|$ of Figure 5a (also seen to persist for a longer time). The evolution of $\mathcal{E}$ in $[0, 2000]$ is shown in Figure 5b. The variation of $\mathcal{E}$ and the persistence of the two unequal peaks at the sites $n = 5$, 8 suggests the possibility of an attracting torus or periodic orbit that is not a breather.

In the case of saturable nonlinearity, *periodic* boundary conditions and vanishing potential the "plane wave" breather solution $u_n = e^{-i\omega t}A$, $n = 1, \ldots, N$, A independent of n, is a global maximum of H over configurations with constant power. We see numerically that this breather also attracts orbits that start far from it. The relation between ω and A depends on the nonlinearity G, and the efficiency of this breather is unity. Note that such solutions are not present for Dirichlet boundary conditions. The attractivity of the plane wave breather is a robust phenomenon, and is observed for many different couplings. In the example of Figures 6a-b we considered a saturable DNLS with the periodic five-point Laplacian, and $N = 17$, $\delta = -0.1$ and $\alpha = 0.1$. In Figure 6a we show $|u_n(0)|$, and $|u_n(100)|$. The trajectory converges to a plane wave breather with the amplitude profile of $|u_n(100)|$. In Figure 6b we show the evolution $\mathcal{E}$ in the time interval $[0, 100]$, i.e. the attracting breather has $\mathcal{E} = 1$. The attracting breather is clearly independent of δ. Larger δ is seen to lead to faster convergence to the breather.

The general idea of adding a power conserving non-Hamiltonian perturbation is independent of

the model and is also applicable to higher dimensional Hamiltonian lattice models with global phase symmetry. The perturbation of (2.26) can be also used for higher dimensional lattices with positive stable breathers. A preliminary step is the enumeration of the sites of the higher dimensional lattice, and it is clear that the property of global phase invariance is independent of this enumeration. On the other hand, sites that are adjacent in the higher dimensional lattice can be far from each other in the equivalent one-dimensional lattice. This fact does not seem to cause any problems. One difficulty with higher dimensional models is that we have less information about the set of breather solutions. Still there are many known real breathers, using e.g. the theory of [14], and we may expect that some of the positive, stable breathers seen in the one dimension may have analogues in higher dimensions. In numerical experiments with a 2-dimensional discrete cubic NLS with nearest neighbor interactions in a 7×7 grid we readily found trajectories converging to positive (hence $\mathcal{E} = 1$) breathers that are analogous to the breathers of Figures 2, 3, and 5. For instance, we used Dirichlet boundary conditions and $\delta = -4.0$ to see convergence to a two dimensional positive breather that is approximately the product of two copies of the shape of Figure 2a. Choosing $\delta = -2.0$, Dirichlet boundary conditions, and a potential V satisfying $V(4,4) = -10$, $V(i,j) = 0$ everywhere else, we see convergence to a positive breather that has its maximum at the site $(4,4)$. In the case of periodic boundary conditions we see trajectories that convergence to a plane wave positive breather with equal amplitudes, i.e. the 2-dimensional analogue of the breather of Figure 5. Such a breather is easily seen to be a a global extremum of the constrained Hamiltonian. The argument holds in any dimension.

The examples of Figures 2a, 3a, 6a suggest that the basin of attraction of the corresponding breathers is extended. There is also some evidence that the basin of attraction of these breathers may be the whole sphere of constant power, at least for the range of powers we considered. Specificaly, we integrated the equations of Figures 2a, 3a, 6a using 100 "pseudo-random" initial conditions with the same respective power and saw that in all cases the trajectories congerged to the respective breathers of Figures 2a, 3a, 6a.

Pseudo-random initial conditions are points in equidistributed sequences. A sequence $\{z_n\}_{n=1}^{\infty}$ on a set Z with measure σ is *equidistributed* if for any $\sigma-$measurable $A \subset Z$ the fraction of points $z_1, \ldots, z_m$ of the sequence that belong to A converges to $\sigma(A)/\sigma(Z)$ as $m \to \infty$, see e.g. [19], ch. 4, and [20], ch. 5.9. Such a sequence can be generated by iterating an ergodic map on (Z, σ), see [19], p.87. In the present case we let X be the power hypersurface $P = Nc$, and σ the microcanonical invariant measure associated to the constant P on the power hypersurface $P = Nc$, see [11], Ch. II, 7. The fact that the changes of coordinates leading to the variables I, θ are symplectic (up to a scaling factor) implies that σ is, up to a constant, the Lebesgue measure μ_{2N-1} on $\mathtt{S}_c^{N-1} \times \mathbf{T}^N \subset \mathbf{R}^{2N-1}$, where $\mathtt{S}_c^{N-1}$ is the set of $[I_1, \ldots, I_{N-1}] \in \mathbf{R}^{N-1}$ that satisfy $J_k > 0$, $k = 1, \ldots, N$, with J_k as in (2.3). (The scaling factor can be avoided by defining the variable J in Section 2 by $u_n = \sqrt{2J_n} e^{i\phi_n}$, $n = 1, \ldots, N$.) Furthermore, the change to the variables $r_k = I_k + kc$, $k = 1, \ldots, N-1$ maps $\mathtt{S}_c^{N-1}$ to $\tilde{\mathtt{S}}_c^{N-1}$, where

$$\tilde{\mathtt{S}}_c^{N-1} = \{[r_1, \ldots, r_{N-1}] \in [0, Nc]^{N-1} : r_1 \leq r_2 \leq \ldots \leq r_{N-1}\}. \tag{3.6}$$

The map from the I_k to the r_k is a translation in $\mathbf{R}^{N-1}$, and preserves the Lebesgue measure μ_{N-1}, therefore it is enough to produce equidistributed sequences $[0, 2\pi]^N \times \tilde{\mathtt{S}}_c^{N-1}$, which is a subset of a rectangle in $\mathbf{R}^{2N-1}$. Note that $\mu_{2N-1}([0, 2\pi]^N \times [0, Nc]^{N-1}) = (N-1)!\mu_{2N-1}([0, 2\pi]^N \times \tilde{\mathtt{S}}_c^{N-1})$, which also means that producing and equidistributed sequence in $[0, 2\pi]^N \times [0, Nc]^{N-1}$, and deleting

the ones outside $[0,2\pi]^N \times \tilde{\mathfrak{S}}_c^{N-1}$ is inefficient for large N. Instead, consider an equidistributed sequence (α_n, β_n), $n = 1, 2, \ldots$ in $[0,2\pi]^N \times [0, Nc]^{N-1}$, and let $G(\alpha_n, \beta_n) = (\alpha_n, s(\beta_n))$, where the map s sorts the components of β_n from smallest to largest. Thus $G(\alpha_n, \beta_n)$, $n = 1, 2, \ldots$, is a sequence in $[0,2\pi]^N \times \tilde{\mathfrak{S}}_c^{N-1}$. Assume that (α_n, β_n), $n = 1, 2, \ldots$ is equidistributed. Let $\tilde{F}_m$ be the fraction of $G(\alpha_n, \beta_n)$, $1, \ldots, m$, in $\tilde{U}$, and let F_m be the fraction of the (α_n, β_n), $1, \ldots, m$, in $G^{-1}(\tilde{U})$. Then

$$\tilde{F}_m = F_m \to \frac{\mu_{2N-1}(G^{-1}(\tilde{U}))}{\mu_{2N-1}([0,2\pi]^N \times [0,Nc]^{N-1})} = \frac{(N-1)!\mu_{2N-1}(\tilde{U})}{(N-1)!\mu_{2N-1}([0,2\pi]^N \times \tilde{\mathfrak{S}}_c^{N-1})}, \tag{3.7}$$

as $m \to \infty$, and therefore $G(\alpha_n, \beta_n)$, $1, 2, \ldots$ is an equidistributed sequence in $[0,2\pi]^N \times \tilde{\mathfrak{S}}_c^{N-1}$. The problem is then reduced (up to rescaling) to that of producing an equidistributed sequence in $[0,1]^{2N-1}$. To do that we can iterate irrational rotations on the $(2N-1)-$torus, i.e. maps $x_j \mapsto (x_j + \omega_j) \mathrm{mod} 1$, $j = 1, \ldots, 2N-1$, where the ω_j, $j = 1, \ldots, 2N-1$, are linearly independent over the integers. In the simulations we chose as ω_j (double precision approximations of) square roots of different prime numbers (see e.g. [20], ch. 5.9.3, and references for this choice), and checked for equidistribution by counting the number of iterates in simple shapes of known volume, e.g. subsets where one of the components is within a subinterval of $[0,1]$, using up to 10^4 iterations.

4 Conclusions

We report results on perturbed Hamiltonian systems for which the addition of a small non-Hamiltonian perturbation provides an attracting region towards a state of high coherence, where coherence is characterized by number $\mathcal{E}$ of (2.21). We also found regimes where the attractor is a spatially localized state. This particular case is reminiscent of the solitary wave one arrives at in continuum complex Landau-Ginzburg systems. Both of these features (high coherence, spatial localization) are currently sought in realistic optical systems. A particularly relevant example that motivated this work is that of fiber laser arrays, where the goal is to obtain highly coherent intense and ideally highly localized field intensity outputs.

Acknowledgments. P. Panayotaros wishes to thank the Department of Mathematics of Southern Methodist University for its hospitality, and A. Olvera for helpful discussions. He also acknowledges partial support by a DGAPA-UNAM stipend. A. Aceves acknowledges the useful collaborations with Dr. Erik Bochove from the Air Force Research Laboratory.

References

[1] D. J. Richardson, J. Nilsson, W. A. Clarkson, "High power lasers: current status and future perspectives [Invited]", J. Opt. Soc. Am. B **27**, B63–B92 (2010)

[2] Y. Huo, P. K. Cheo, "Analysis of transverse mode competition and selection in multicore fiber lasers", JOSA B **22** 2345–2349 (2005)

[3] A. Mafi, J. V. Moloney, "Phase locking in a passive multicore photonic crystal laser", JOSA B **21** 897–902 (2004)

[4] S. Peles, J. Rogers, K. Wiesenfeld, "Robust synchonization in fiber laser arrays", Phys. Rev. E. **73**, 026212 (2006)

[5] T. Wu, W. Chang, A. Galvanuskas, H. Winful, "Model for passive coherent beam combining in fiber laser arrays", Opt. Exp. **17** 19509–19518 (2009)

[6] D. Kouznetsov, J. F. Bisson, A. Shirakawa, K. Ueda, "Limits of Coherent Addition of Lasers: Simple Estimate", Optical Review **12** 445–447 (2005)

[7] E. J. Bochove, P. K. Cheo, G. G. King, "Self-organization in a multicore fiber laser array", Opt. Lett. **28** 1200–1202 (2003)

[8] Y. Kuramoto, *"Chemical Oscillations, Waves and Turbulence"*, Dover, New York (1984)

[9] V. Eckhouse, M. Fridman, A. Friesem, "Loss Enhanced Phase Locking in Coupled Oscillators", Phys. Rev. Lett. **100**, 024102 (2008)

[10] R. Abraham, J. Marsden, *"Foundations of Mechanics"*, W.A. Benjamin, Reading (1978)

[11] A.I. Khinchin, *"Mathematical foundations of Statistical Mechanics"*, Dover, New York (1949)

[12] D. N. Christodoulides, R. I. Joseph, "Discrete self-focusing in nonlinear arrays of coupled waveguides", Opt. Lett. **18**, 794 (1988)

[13] J. C. Eilbeck, P. S. Lomdahl, A. C. Scott, "The discrete self-trapping equation", Physica D **16**, 318–338 (1985)

[14] R. S. MacKay, S. Aubry, "Proof of existence of breathers for time-reversible or Hamiltonian networks of weakly coupled oscillators", Nonlinearity **7**, 1623–1643 (1994)

[15] J. Milnor: *"Morse theory"*, Princeton University Press, (1973)

[16] P. Panayotaros, "Continuation and bifurcation of breathers in a finite discrete NLS equation", Disc. Cont. Dyn. Syst. S 4, **5**, 1227–1245 (2011)

[17] P. Panayotaros, "Instabilities of breathers in a finite NLS lattice", preprint (2011)

[18] D. E. Pelinovsky, P. G. Kevrekidis, D. J. Frantzeskakis, "Stability of discrete solitons in nolinear Schrödinger lattices", Physica D **212**, 1–19 (2005)

[19] M. Brin, G. Stuck, *"Introduction to Dynamical Dystems"*, Cambridge Univesity Press, Cambridge (2002)

[20] P.J. Davis, P. Rabinowitz, *"Methods of numerical integration"*, 2nd. Ed., Academic Press, Olrlando (1984)

Figure Captions.

Fig. 1: Contour plot for the reduced Hamiltonian h_c of the 2−site cubic DNLS, $\delta = -1.2$.

Fig. 2a: $|u_n|$ vs. site number n at times $t = 0$ (boxes), and $t = 100$ (connected discs), saturable DNLS, Dirichlet B.C., $N = 17$, $\delta = -5.1$.

Fig. 2b: $\mathcal{E}$ vs. time t for a trajectory with the initial condition of Fig. 2 (upper curve, initial $\mathcal{E} = 0.985306583$), and for a trajectory with initial $\mathcal{E} = 0.528646241$ (lower curve).

Fig. 3a: $|u_n|$ vs. site number n at times $t = 0$ (boxes), and $t = 200$ (connected discs), saturable DNLS with potential $V(9) = -10$, zero elsewhere, Dirichlet B.C., $N = 17$, $\delta = -5.1$.

Fig. 3b: $\mathcal{E}$ vs. time t for trajectory with the initial condition of Fig. 3a.

Fig. 4a: $|u_n|$ vs. site number n at timse $t = 0$ (boxes), and $t = 1200$ (connected discs), saturable DNLS, Dirichlet B.C., $N = 9$, $\delta = -0.2$.

Fig. 4b: $\mathcal{E}$ vs. time t for trajectory with the initial condition of Fig. 4a.

Fig. 5a: $|u_n|$ vs. site number n at times $t = 0$ (boxes), and $t = 2000$ (connected discs), saturable DNLS, Dirichlet B.C., $N = 9$, $\delta = -0.2$

Fig. 5b: $\mathcal{E}$ vs. time t for trajectory with the initial condition of Fig. 5a.

Fig. 6a: $|u_n|$ vs. site number n at times $t = 0$ (boxes), and $t = 100$ (connected discs), saturable DNLS, periodic B.C., $N = 17$, $\delta = -0.1$.

Fig. 6b: $\mathcal{E}$ vs. time t for a trajectory with the initial condition of Fig. 6a.

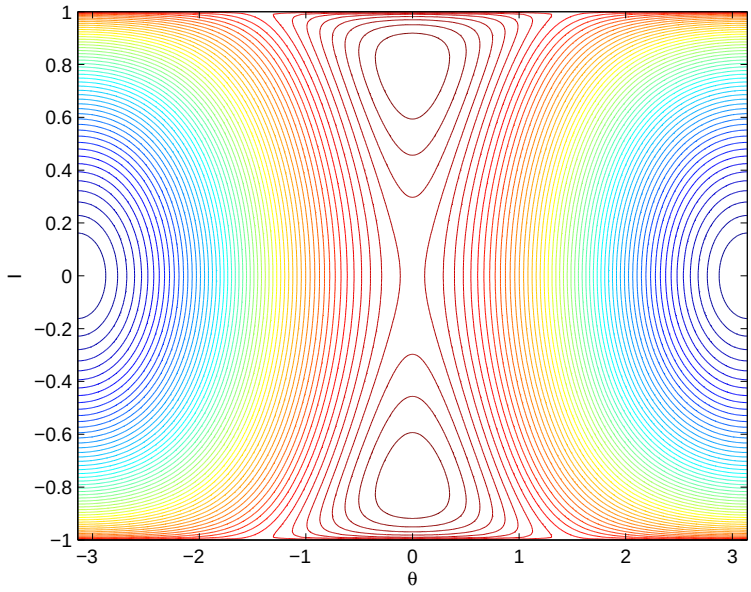

Figure 1

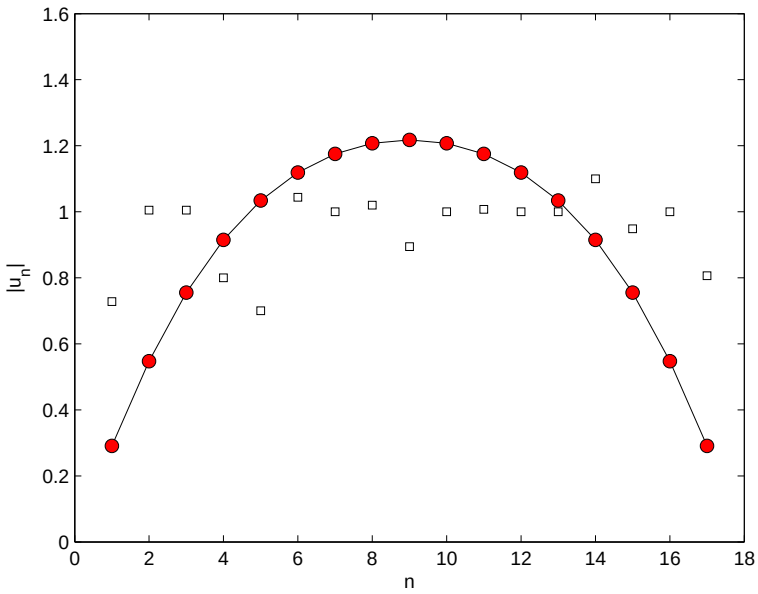

Figure 2 a

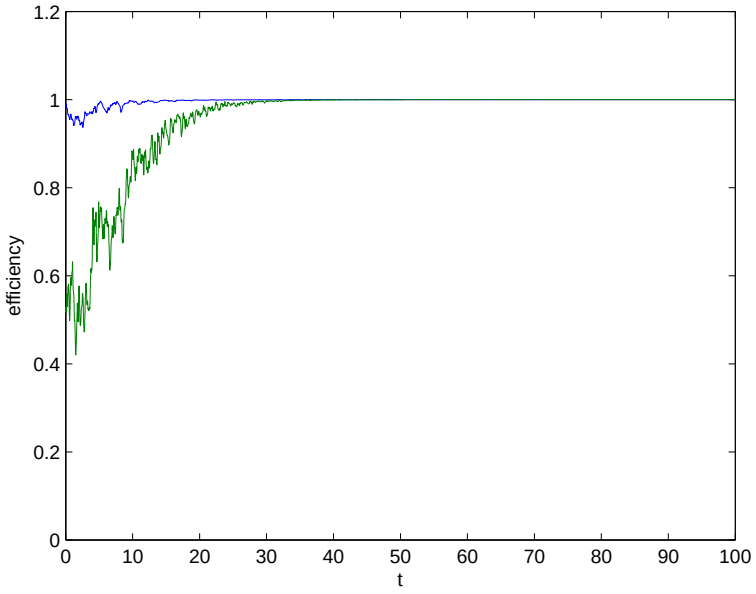

Figure 2 b

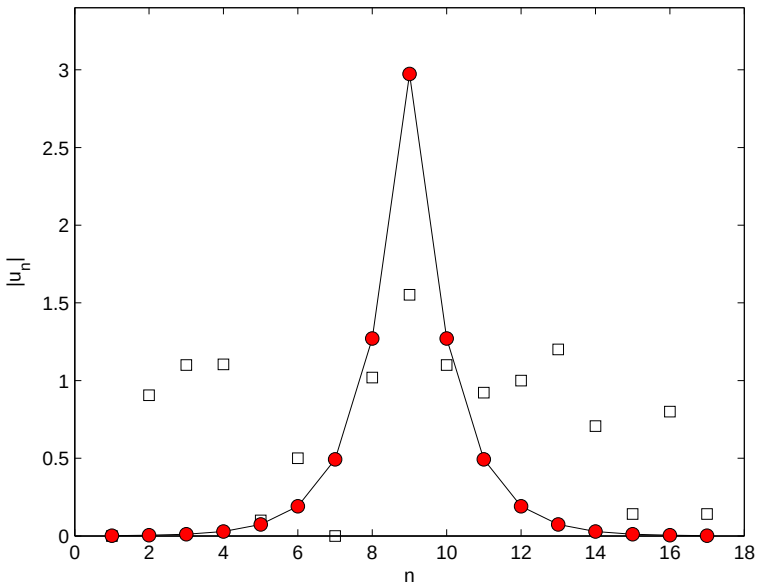

Figure 3 a

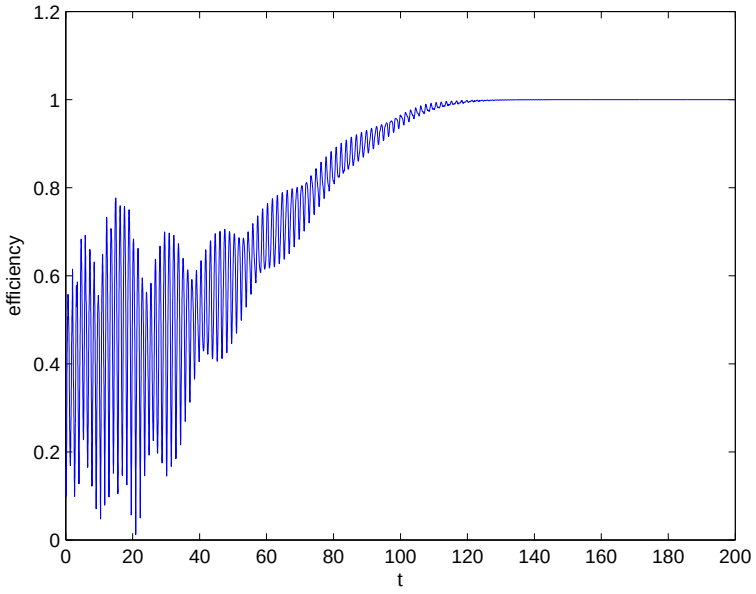
1.2
1
0.8
0.6
0.4
0.2
0
efficiency
0
20
40
60
80
100
120
140
160
180
200
t

Figure 3 b

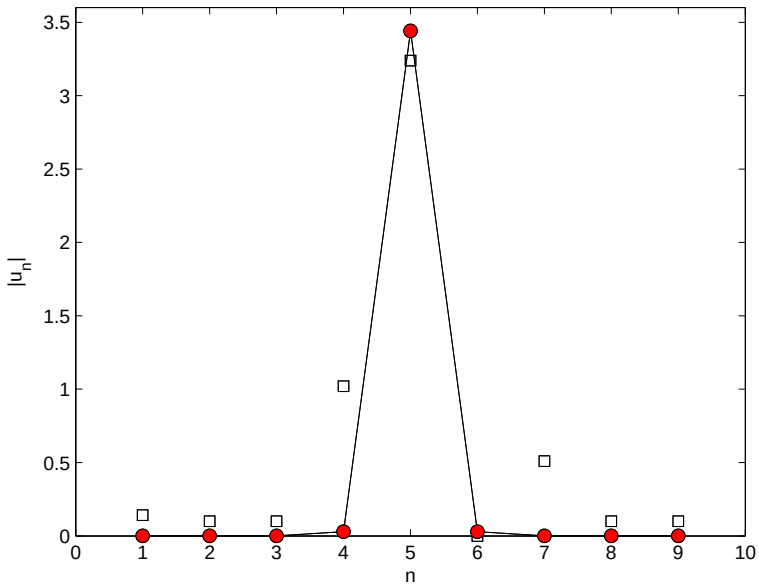

Figure 4 a

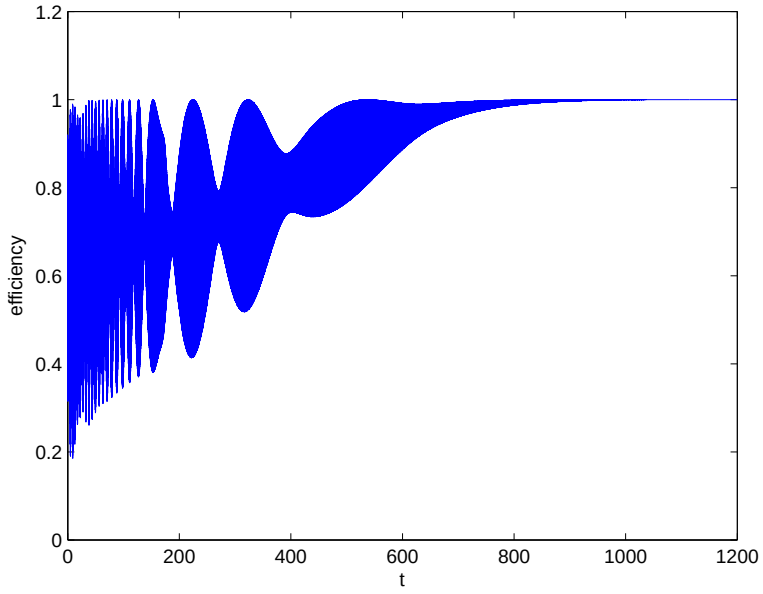

Figure 4 b

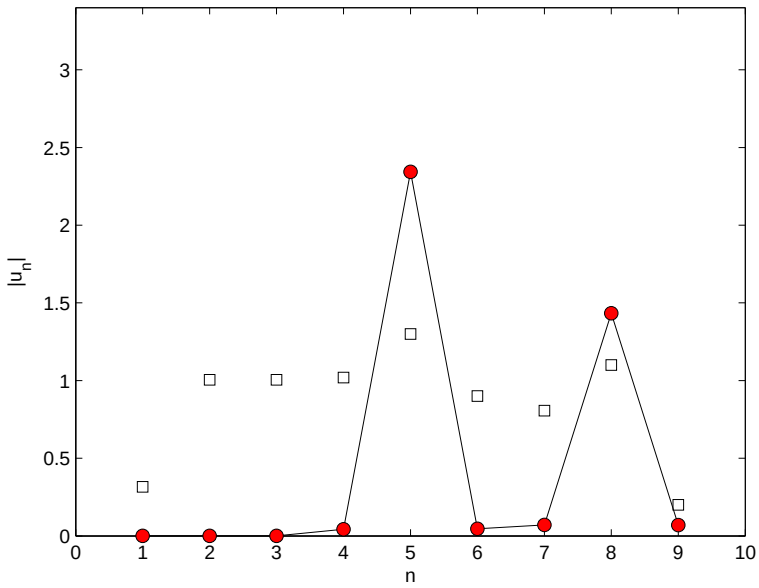

Figure 5 a

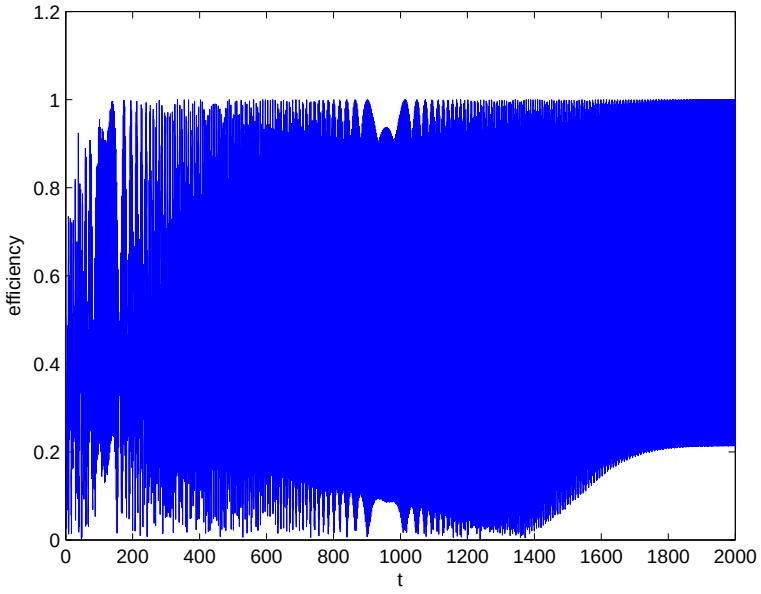
1.2
1
0.8
0.6
0.4
0.2
0
efficiency
0
200
400
600
800
1000
1200
1400
1600
1800
2000
t

Figure 5 b

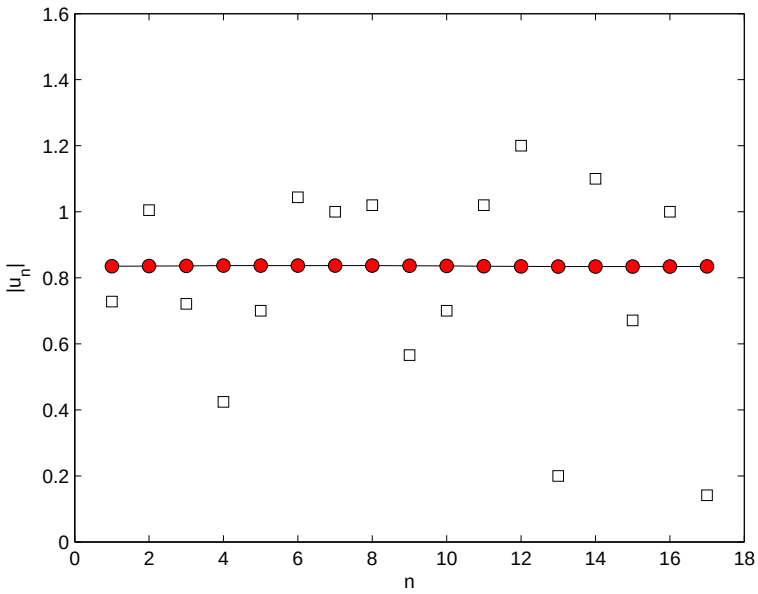

Figure 6 a

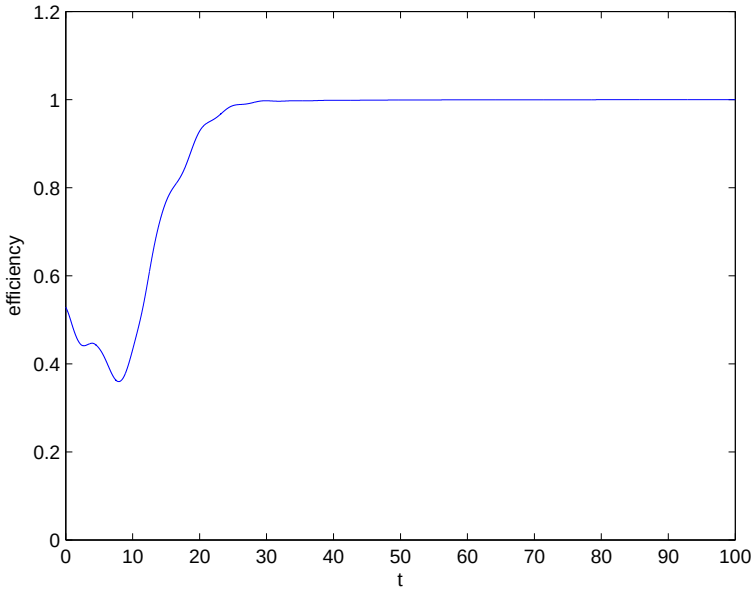

Figure 6 b